PAPER • OPEN ACCESS

Particle transport modelling for D/T ratio control experiments in JET

To cite this article: K.K. Kirov *et al* 2025 *Nucl. Fusion* **65** 106016

OPEN ACCESS
IOP Publishing | International Atomic Energy Agency
Nuclear Fusion
Nucl. Fusion **65** (2025) 106016 (19pp)
https://doi.org/10.1088/1741-4326/ae00da

Particle transport modelling for D/T ratio control experiments in JET

K.K. Kirov[1,*], M. Lennholm[1], L. Piron[2,3], D. Valcarcel[1], P. Almond[1], M. Baruzzo[3,4,5], M. van Berkel[6], T. Bosman[6,7], L. Ceelen[6,7], P. Fox[1], L. Garzotti[1], Z. Ghani[1], B. Kool[6,7], C. Lowry[1], J. Mitchell[1], B. Sieglin[8], H. Sun[1], JET contributors[a] and the EUROfusion Tokamak Exploitation Team[b]

EUROfusion Consortium, JET, Fulham Science Centre, Abingdon OX14 3DB, United Kingdom of Great Britain and Northern Ireland

[1] United Kingdom Atomic Energy Authority, Fulham Campus, Abingdon, Oxon OX14 3DB, United Kingdom of Great Britain and Northern Ireland
[2] Dipartimento di Fascia 'G. Galilee', University deli Study di Pad ova, Pad ova, Italy
[3] Consorzio RFX, Coors State Unity 4, 35127 Pad ova, Italy
[4] Fusion and Nuclear Safety Department, ENEA, C.R. Fractal, Rome, Italy
[5] ENEA Fractal, C.P. 65, 00044 Fractal, Italy
[6] DIFFER—Dutch Institute for Fundamental Energy Research, De Zaale 20, 5612 AJ Eindhoven, Netherlands
[7] Department of Mechanical Engineering, Control Systems Technology Group, Eindhoven University of Technology, Eindhoven, Netherlands
[8] Max Planck Institute for Plasma Physics, Boltzmannstr. 2, 85748 Garching, Germany

E-mail: Krassimir.Kirov@ukaea.uk

Received 7 May 2025, revised 13 August 2025
Accepted for publication 29 August 2025
Published 12 September 2025

Abstract

This study presents results from particle transport modelling for D/T ratio control experiments conducted during the JET DTE3 campaign. TRANSP interpretative and JETTO predictive simulations for D and T densities were performed and their results are discussed. Despite using simplified models based on Bohm-gyroBohm transport, the simulations incorporate self-consistent sources and impurities and cover the full radial range. The simplified models effectively reproduced the evolution of electron density and neutron rates. However, the predicted D/T ratio evolution responded to control requests faster than what was experimentally observed, suggesting that the employed models possess certain limitations. Specific cases involving swapped gas injection species were also studied, highlighting the potential applicability of the proposed methodology in future experimental scenarios. TRANSP interpretative analysis indicates that a Real-Time (RT) scheme employing simplified quasi-neutrality and Z_{eff} estimations can be implemented with high degree of reliability. JETTO predictive analysis suggests that a simplified modelling approach for the behaviour of the future

[a] See Maggi *et al* 2024 (https://doi.org/10.1088/1741-4326/ad3e16) for JET Contributors.
[b] See Joffrin *et al* 2024 (https://doi.org/10.1088/1741-4326/ad2be4) for the EUROfusion Tokamak Exploitation Team.
[*] Author to whom any correspondence should be addressed.

RT controllers of D/T mixture can be effective. Such an approach involves using measured temperatures, omitting explicit modelling of the SOL physics, and adopting simplified assumptions for the particle transport.

Keywords: D/T ratio, DT experiments JET, particle transport, modelling

(Some figures may appear in colour only in the online journal)

1. Introduction

Controlling the deuterium/tritium (D/T) ratio in future fusion experiments is crucial for optimising the fusion performance. DT fusion rate per unit volume dR_{DT}/dV is proportional to the densities of the reactants, n_D for D and n_T for T ions, as well as the averaged reactivity, $\langle\sigma v\rangle$, i.e. $dR_{DT}/dV = n_D n_T \langle\sigma v\rangle$. Figure 1(*a*) illustrates the sensitivity of the reaction rates to the D/T mixture for thermonuclear reactions as shown by dashed red lines. Ideally, the maximum thermonuclear fusion rate occurs for D/T ratio of 0.5/0.5. Furthermore, it is noteworthy that for D/T ratios between 0.4/0.6 and 0.6/0.4 the reduction in reaction rate is relatively small—approximately 4%. However, further imbalance, such as D/T ratio of 0.3/0.7, significantly impacts fusion performance, reducing the rate by 16%. A D/T ratio of 0.25/0.75, results in a 25% drop, highlighting the necessary of maintaining D/T close to 0.5/0.5 in future operations.

In most of the existing fusion reactors featuring neutral beam injection (NBI), such as JET, a significant fraction of fusion reactions occurs through so-called Beam-Target (BT) collisions. As shown by the black line in figure 1(*a*), which represents dR_{DT}/dV for the sum of both thermal and BT reactions, it is evident that even in the case when BT reactions dominate over thermonuclear ones, fusion performance is maximised at a specific D/T ratio, which is different from thermonuclear maximum at 0.5/0.5. For example, in the case shown in figure 1(*a*) the maximum performance for thermal and BT reactions occurs at approximately D/T $\approx$ 0.4/0.6. A similar trend is observed in figure 1(*b*), which depicts the measured total fusion rate under real experimental conditions. Maintaining this ratio would be highly desirable for optimising the overall fusion yield in this scenario.

Recent JET DTE2 campaigns [1] have focused on developing scenarios with distinct characteristics in terms of confinement and operational space, including the baseline [2, 3] and hybrid [4, 5] scenario as well as scenario dominated by BT rates, known as T rich scenario [6]. Optimising D/T ratio was a key requirement for all these scenarios, necessitating additional experimental time. Notably, while for baseline scenario the fusion performance is governed by thermal reactions the optimal D/T ratio remained close to 0.5/0.5; the T rich scenario with dominant BT rates required a significantly different D/T ratio of approximately 0.1/0.9 for optimal performance. Throughout these optimisation studies, it became evident that precise control of D/T ratio via feedback (FB) control could offer substantial benefits in improving the optimisation process.

One of the objectives of the JET DTE3 campaign was to develop real-time (RT) controllers for the future fusion reactors, with a particular focus on a reliable RT controller for D/T ratio control. For the first time, this campaign successfully demonstrated [7–10] active D/T ratio control using a FB system. During these experiments, several challenges related to particle sources, e.g. delays in gas introduction system response, hysteresis in gas injection modules, missing pellets, strong dependence of NBI deposition on density, etc. which subsequently affected our understanding of the transport, were identified as crucial factors affecting the reliability of D/T control RT system. Addressing these issues is essential for improving the performance of the RT system. Similar challenges are expected in near-future fusion machines such as ITER [11, 12] and SPARC [13] as well as in more advanced projects like DEMO [14] and STEP [15, 16].

Fuelling thermonuclear plasma with D and T reactants can be modelled in a fluid approximation by the well-known transport codes e.g. JETTO [17], TRANSP [18, 19]. These codes incorporate all the essential building blocks: particle sources and losses, particle transport and fusion reactions. Various contributions to D and T density profiles arise from transport processes like conduction and convection as well as particle sources and sinks. Additionally, fusion reactions should be accurately accounted for, as they contribute to D and T losses, He ash accumulation and plasma heating by alphas. Particle transport has been intensively studied [20–24]. Regarding particle sources, there are three primary methods for fuelling fusion plasma: gas puff and recycling, NBI and pellet injection. These methods differ significantly in terms of spatial and energy distribution of the particle sources. Gas injection modules are placed at various points along the plasma periphery. The gas they inject is ionised near the plasma boundary and, through processes such as advection and inward pinch D/T ions penetrate into hot plasma core. In contrast, pellets provide deeper particle deposition. NBI involves injecting energetic neutral particles deep into the plasma core, where they are ionised and converted into fast ions that slow down to energies of the order of the ion temperature, thereby supplying continuous source of thermal ions in the core.

A better understanding of the sources and particle transport is essential for effective DT ratio control. Future reactors will require accurate estimates of these sources and transport coefficients to optimise fuelling and enable corrective actions when necessary. The peripheral particle sources provided by gas injection and pellets, rely on transport processes to deliver D and/or T ions to the plasma core. The time constants of these processes are of the order of particle confinement times,

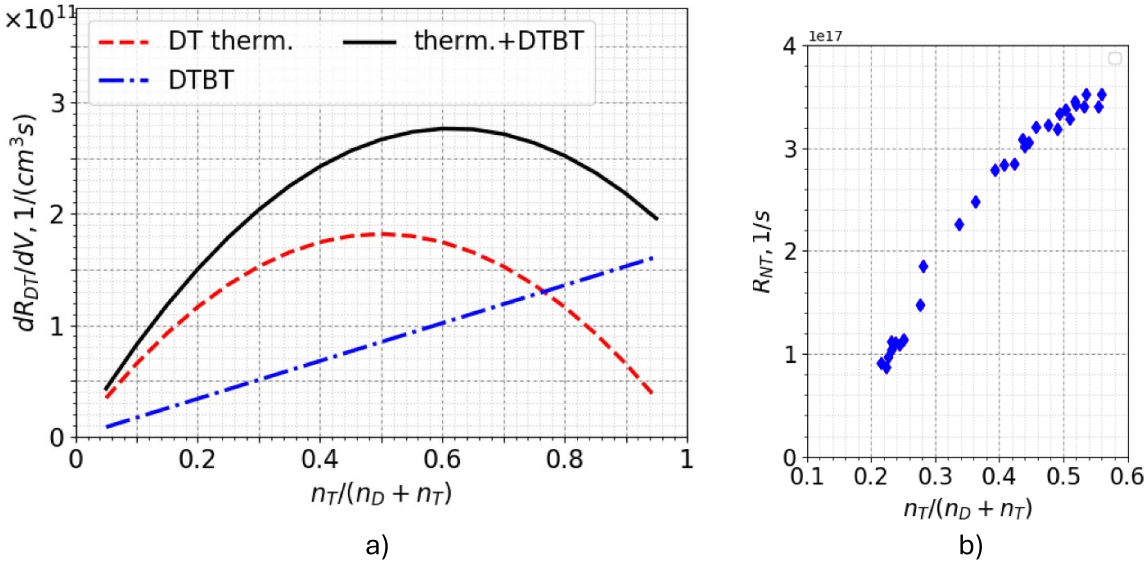

Figure 1. (*a*). Reaction rates $\mathrm{d}R_{\mathrm{DT}}/\mathrm{d}V$ vs. D/T ratio, $n_{\mathrm{T}}/(n_{\mathrm{D}}+n_{\mathrm{T}})$, for thermal fusion (DT therm., dashed red line), D beam on T target plasma ions (DTBT, dashed-dotted blue line) and the sum of thermonuclear and beam-target (therm.+ DTBT, black line) for JET DTE conditions, $n_{\mathrm{e}} = 8\times10^{19}$ m^{-3} ($n_{\mathrm{D}}+n_{\mathrm{T}}=n_{\mathrm{e}}$) and $T_{\mathrm{e}}=T_{\mathrm{i}}=10$ keV. (*b*). Measured total neutron rate, $R_{\mathrm{NT}}=\int(\mathrm{d}R_{\mathrm{DT}}/\mathrm{d}V)\,\mathrm{d}V$, versus measured $n_{\mathrm{T}}/(n_{\mathrm{D}}+n_{\mathrm{T}})$ ratio in JET DTE pulse #104651.

ranging from several hundred milliseconds to few seconds, which makes D/T ratio control on fast timescales particularly challenging. It is also possible that edge transport barrier (ETB) in H-mode plasmas could significantly limit the fuelling efficiency of gas injection modules, reducing the penetration of edge ions in the core. In contrast, pellets provide direct penetration into the plasma, which means the time scales of typical D/T ratio control would generally need to be faster in this case. Different particle sources exhibit varying characteristic times for central penetration. As a result, more sophisticated D/T ratio controllers in the future will need to account for these time characteristics when setting RT feedback parameters.

The aim of this study is to assess whether simplified transport models reasonably predict the behaviour of real time D/T ratio controllers. Specifically, we use a simplified approach to model D/T ion transport, relying on the well-known semi-empirical Bohm-gyroBohm (BgB) transport in a coupled, self-consistent, source driven full radius model. The importance of D/T ion sources and sinks has been emphasised and efforts have been made to model these as accurately as possible under experimental conditions. Predicting the thermal energy transport is not included in this study, as electron and ion temperature are assumed to be available from measurements. While this assumption might seem inconsistent with full self-consistent simulations across all transport channels, it is deemed sufficient for the purposes of RT control testing simulator. Indeed, there is no reason to believe that future RT control tools will not be able to process temperature data as input. After demonstrating the applicability of these simplified models, they can be used to numerically investigate key issues related D/T ratio control. These include (i) the impact of different particle sources on D/T ratio control and (ii) determining which inputs to the RT controller—such as gas injection rates, the measured D/T ratio, neutron yield or combinations of these—should be prioritised in the development of effective DT ratio control schemes.

This paper presents the results of particle modelling for D/T ratio control experiments conducted on JET during DTE3 campaign. The main conclusion from this study is that predictive modelling codes can be successfully applied to model the physics of particle transport for the future D/T ratio control experiments. This paper is organized as follows: section 1 details the codes used in the study and outlines key aspects of the analysis. Section 2 describes the experimental setup, the diagnostics employed, and a brief summary of the pulses in the D/T ratio control experiments. Section 3 presents the results of the modelling analysis, while section 4 concludes the paper with a summary of key findings.

2. Details of modelling analysis

2.1. Description of the numerical tools used in the study

The TRANSP [18, 19] code was used in the analysis presented here owing to its accurate prediction of NBI sources and fusion rates. Neutral beam deposition and fuelling in TRANSP were calculated by NUBEAM code [25] which is a computationally comprehensive Monte Carlo (MC) code for NBI heating in tokamaks. Gas injection modelling in TRANSP is performed by means of FRANTIC code [26].

Routine predictive transport modelling at JET is usually performed with the JETTO code [17, 27] coupled to PENCIL [28, 29] or ASCOT [30] package for computing NBI power and particle sources. Various transport models can be used

in JETTO based on first principles physics or empirical scaling. A distinctive semi-empirical model which gives reasonable agreement with a large proportion of JET experimental data is the BgB model [31], which uses combination of Bohm and gyro-Bohm terms in the heat diffusivity expression. Gas injection in JETTO is modelled by FRANTIC code [26], although JETTO implementation is different from TRANSP. Pellet modelling in JETTO can be done by means of one of the available three models: continuous pellets [32], Neutral Gas and Plasma Shielding model [33] and HPI2 model [34].

One significant advantage in using JETTO in our studies is its well-developed feedback control capabilities [32]. The implementation of a new feedback control scheme based on D/T ratio optimisation can be seamlessly integrated into JETTO. Therefore, once the code's ability to model the experiments is validated, which is the main goal of this study, we can propose upgrades to incorporate D/T ratio control.

2.2. Factors influencing D/T ratio control

An essential part of the analysis involves modelling transient phases during which D and T sources undergo significant modification. The transition to a different mixture ratio, along with the associated transient events, presents a challenging task that require careful consideration of particle sources and transport. Currently, most well established particle transport models focus on steady-state phases of experiments [35–37] while research on the fuel mixing process and transient events [23, 38, 39], remains in its early stages.

The analysis must also incorporate transport in the edge pedestal and account for gas injection rates. These additional requirements introduce further complexity compared to previous modelling efforts, which focus solely on core transport while overlooking pedestal dynamics, sources and gas introduction physics [36, 37]. The importance of the pedestal in understanding the mixing of hydrogenic isotopes in plasma was recently highlighted in [35, 40].

Understanding particle sources and transport is crucial in this analysis. Therefore, a brief summary of recent advances in this field is presented here.

2.3. Particle transport: core fluxes and edge barrier

Core particle transport has been extensively documented in numerous publications, including but not limited to [11, 12, 20, 41–43]. Over the years, extensive JET studies have also been conducted and published [21–24, 35, 44, 45]. The key conclusion from these studies is that particle transport on JET is predominantly anomalous and driven by ITG turbulence.

Summarised in a simplified form, the cross field diffusion coefficient, D, and heat diffusivity, χ, for drift-wave turbulence scales as [46] $D \approx \chi \approx \Delta_r^2/\delta t$ where the turbulence characteristic time scale is given by $\delta t \approx L_\theta/v_d \approx L_\theta/(T/eZBL_r)$. Here, L_θ represents the poloidal scale length, v_d is the drift velocity and L_r corresponds to the radial profile gradient length for density, L_n, or temperature, L_T. The term, Δ_r, in the expression above denotes the characteristic turbulent radial scale length. This leads to the transport coefficients $D \approx \chi \approx (T/eZB)\,\Delta_r^2/L_\theta L_r$. Depending on how the turbulent radial scale length Δ_r is assessed, different diffusion models arise: (i) Bohm type diffusion occurs when Δ_r scales with the plasma size, i.e. the minor radius $\Delta_r \approx a$, or (ii) gyro-Bohm type of diffusion occurs when Δ_r is proportional to the ion Larmor radius, i.e. $\Delta_r \approx \rho_i$. The Bohm and gyro-Bohm models [31] implemented in JETTO provide estimates for electron and ion heat diffusivities as follows:

$$\chi_e = \chi_{e,B} + \chi_{e,gB},\ \chi_i = \chi_{i,B} + \chi_{i,gB} \tag{1}$$

where:

$$\chi_{e,B} = \alpha_B \frac{a}{B_t}\frac{T_e}{L_{p_e}} q^2 \left(\frac{T_e(\rho_{\rm int}) - T_e(\rho_{\rm ped})}{T_e(\rho_{\rm ped})}\right);\ L_{p_e} = \frac{p_e}{|\partial p_e/\partial\rho|};$$
$$\alpha_B = 8\times10^{-5};\ \chi_{i,B} = 2\chi_{e,B} \tag{2}$$

$$\chi_{e,gB} = \alpha_{gB}\frac{T_e^{1/2}}{B_t^2}\frac{T_e}{L_{T_e}};\ L_{T_e} = \frac{T_e}{|\partial T_e/\partial\rho|};\ \alpha_{gB} = 5\times10^{-6};$$
$$\chi_{i,gB} = 0.5\chi_{e,gB} \tag{3}$$

and the non-local factor $\left(\frac{T_e(\rho_{\rm int})-T_e(\rho_{\rm ped})}{T_e(\rho_{\rm ped})}\right)$ is calculated at the foot of the pedestal $\rho_{\rm ped}$ near plasma boundary and at $\rho_{\rm int}$ which is about 0.1 m inside $\rho_{\rm ped}$. The particle diffusion coefficients for D and T ions can be defined as proportional to the heat diffusivities, using two coefficients to specify values at the axis and the edge [21, 47]:

$$D_j = \xi_j(\rho)\,\frac{\chi_e\chi_i}{\chi_e+\chi_i},\ \xi_j(\rho) = A_{j,1} + (A_{j,2} - A_{j,1})\,\rho, \tag{4}$$

where j = D, T and $A_{\rm j,1}$, $A_{\rm j,2}$ are constants that can be independently assigned for D and T species. The pinch velocity can be set up proportional to $D_{\rm j}$ or $D_j\nabla T_i/T_i$:

$$\Gamma_j^{\rm inw} = \alpha_i^{\rm inw}\frac{D_j}{V'}\frac{S^2}{V}n_j \text{ or } \Gamma_j^T = \alpha_i^T D_j\frac{\nabla T_i}{T_i}n_j \tag{5}$$

where the latter expression accounts for the thermo-diffusion contribution to particle pinch. The mixed BgB model has been extensively tested on large number of devices and different scenario in both L-mode and H-mode plasma [21, 31, 47, 48]. In the current version of the JETTO code, conductive particle transport for D and T ions can be configured separately through the coefficients $A_{\rm j,1}$ and $A_{\rm j,2}$. However, the convective particle flux coefficients cannot be specified independently for D and T ions, as only a single coefficient $\alpha_i^{\rm inw}$ or α_i^T is available to control the fluxes $\Gamma_j^{\rm inw}$ or Γ_j^T. In the studies discussed here notations A_1, A_2 will be used for the cases when same particle transport coefficients for D and T ions are used, i.e. $A_{\rm D,1} = A_{\rm T,1} = A_1$ and $A_{\rm D,2} = A_{\rm T,2} = A_2$.

As seen from equations (2) and (3), several factors influence the transport of D and T ions. The pedestal height, $a/L_{\rm pe}$, $a/L_{\rm Te}$ all play a role in determining transport behaviour. Additionally, there is an implicit dependence on plasma composition mass through $\chi_{e,gB} \propto M^{1/2}$. In our studies the normalised gradient lengths vary between 5% and 15% for

a/L_{pe} and 5%-20% for a/L_{Te} for different phases and pulses as shown in table 1. For the JET pulses discussed here, which are dominated by ITG turbulence, gyro-Bohm scaling with mass is expected in the collisionless limit. However, several mechanisms—such as collisions, ExB shear flow, and other turbulence regulation processes—can alter the mass dependence of transport coefficients, potentially deviating from the gyro-Bohm scaling.

A crucial aspect of our analysis is understanding the physics governing particle transport, particularly potential differences in D and T ion fluxes in a mixed D/T plasma. This issue is further emphasized by the fact that while a vast database of pure D plasma experiments exists, relatively few experiments have been conducted with D/T mixtures.

The primary challenge in analysing heat and particle transport in mixed D/T plasma lies in determining how transport scales with plasma composition mass. The dependence of transport coefficients—and consequently, confinement—on the effective mass $M_{\mathrm{eff}} = (2^{*}\mathrm{n_D} + 3^{*}n_{\mathrm{T}})/(n_D + n_{\mathrm{T}})$ is often referred to as isotope effects. In our studies, varying the D/T ratio from D/T $\approx$ 0.77/0.23–0.44/0.56 (see table 1) increases the effective mass from $M_{\mathrm{eff}} = 2.23$–2.56, an increase of approximately 15%. This relatively small increase in M_{eff} observed in D/T ratio control experiments is unlikely to significantly impact thermal confinement if one considers the IPB98(y,2) scaling law [11], $\tau_E^{\mathrm{th}} \propto M_{\mathrm{eff}}^{0.2}$. Under this scaling, the expected deviation in τ_E^{th} is less than 3%. However, a major challenge arises due to the lack of consensus among different studies regarding the exact exponent α_M in the $M_{\mathrm{eff}}^{\alpha_M}$ scaling of τ_E^{th}. Experimentally results from TFTR suggest $\alpha_M = 0.89 \pm 0.20$ [49], whereas early JET experiments indicate an even negative exponent, $\alpha_M = -0.25 \pm 0.22$ [50], for the global confinement time and $\alpha_{M,\mathrm{core}} = -0.16 \pm 0.1$ for the core energy confinement after separating core and pedestal energies. Similar scaling has been predicted by TGLF-SAT2 modelling of JET DTE2 pulses [35].

In general, core-edge coupling must be considered in cases where pedestal parameters are evolving. A key example of this nonlinear interaction occurs when improved core confinement leads to an increase in pedestal pressure. This, in turn, can influence edge stability through the well-known β stabilization of peeling–ballooning modes, ultimately modifying pedestal parameters.

2.4. SOL and sources

Accurate modelling of gas injection from gas-injecting modules requires proper treatment of scrape-off layer (SOL) physics. On JET, this can be achieved using the 2D SOL code EDGE2D [51], which solves the 2D fluid equations for the conservation of energy, parallel momentum, and particle transport in the plasma edge region. The model includes ions, electrons, and all ionization stages of multiple species, while gas injection sources can be defined on a discrete poloidal mesh. To simulate interactions with vessel walls, EDGE2D is coupled with the MC code EIRENE [52] which provides neutral ion sources from recycling and gas injection, as well as impurity sources from sputtering. The neutral source profiles generated by EDGE2D can be directly input into JETTO, enabling fully self-consistent plasma-SOL modelling via the 2D MC neutral code EIRENE within the COCONUT workflow [53, 54].

In JETTO, neutral sources can be modelled using either the FRANTIC or EIRENE codes. While EIRENE offers a more advanced treatment of neutrals based on the MC technique, with the added benefit of poloidally localized source definitions, its current implementation in JETTO does not support operation in multi-species plasmas when coupled with SANCO [55]. On the other hand, FRANTIC provides a more simplified approach. Although it lacks the ability to resolve 2D neutral sources in the SOL, it can still deliver reasonably accurate neutral sources at the separatrix and within the edge region. In addition, JETTO simulations with FRANTIC were successfully utilised in developing the fuel mix control of the baseline scenario in DT with D/T gas injection and D pellets [56]. However, FRANTIC's consistency with experimental gas injection rates is somewhat limited. Our findings indicate that, in general, gas injection rates lower than measured values need to be specified, and the neutral temperature must be set lower than the separatrix temperature for FRANTIC to produce realistic gas injection source profiles.

In this manuscript, we consider three primary fuelling sources: gas injection, NBI, and pellets. Figure 2 illustrates the estimated magnitudes of these sources. The NBI source, figure 2(a), is centrally located but contributes relatively little to fuelling, being at least an order of magnitude lower than both gas injection, figure 2(b), and pellet injection, figure 2(c). The latter two sources, being predominantly peripheral, experience reduced transport in the ETB region. In cases of a strong ETB, gas fuelling can become almost negligible due to suppressed edge transport. However, in the pulses examined in this study, the pedestal barrier is not particularly strong, allowing gas injection modules to provide a reasonable fuelling contribution.

2.5. Simplifications adopted in analysis

In proposed analysis the thermal transport is not modelled. However, this limitation should not pose a significant issue for the development of RT D/T ratio controllers, as direct measurements of electron and ion temperatures can be readily incorporated into future RT control schemes. For instance, JET already employs central T_{e} measurements in various RT control algorithms, such as T_{e} hollowness in hybrid pulses [4, 5]. While implementing ion temperature measurements in RT controllers may be more challenging, several studies have demonstrated that T_{i} can be scaled from T_{e} measurements. Future RT D/T ratio control schemes would take inputs such as X[T] (or X[D]), n_{e}, T_{e}, potentially T_{i}, the input heating power, and/or $\mathrm{R_{NT}}$. With these RT signals available, rapid calculations can be performed to determine the necessary D/T ratio adjustments for optimizing fusion performance.

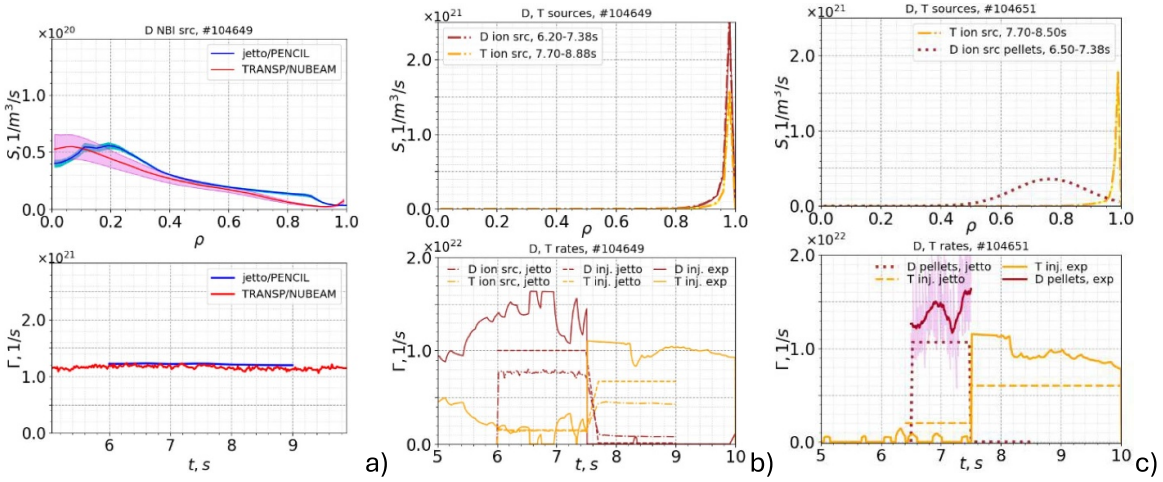

Figure 2. (*a*) D ion sources due to NBI for JET pulse #104649 averaged (solid line) and their evolution shown by one standard deviation (shaded area) over high performance time interval. JETTO simulations between 6.5–8.5 s are shown for PENCIL code (blue), while TRANSP predicted D ion source in 4–11 s interval are from NUBEAM code (red). Profiles are shown in the top graph while time evolution of the total source integrated over plasma volume is shown at the bottom. (*b*) D and T ion sources due to gas injection for JET pulse #104649. (*c*) D and T ion sources due to D pellets (dotted brown lines) and T gas injection (orange lines) for JET pulse #104651. In (*b*) and (*c*) particle sources by JETTO code are again shown in the top, while volume integrated sources are shown at the bottom graphs. Total ion sources (dash-dotted lines) for D (brown) and T (orange), and gas puff used in JETTO/FRANTIC (dashed lines) are compared to real gas injection rates (solid lines).

RT controllers cannot rely on comprehensive transport models due to the computational complexity of the latter. Even the simplest transport models would be impractical for RT implementation, as they would introduce unnecessary delays and uncertainties. Instead, direct measurements provide a far more accurate and faster input for RT control schemes. A very simplified real time models constrained by comparison to limited available measurements is likely to be the way forward.

In the cases studied here, pedestal pressure remains unchanged during variations in the D/T ratio, allowing us to treat the core and the edge independently. JETTO uses an empirical model that incorporates a prescribed ETB width and multiplication coefficients (scale factors) to account for reduced transport in the barrier region. The width of the transport barriers is inferred from High-Resolution Thomson Scattering (TS) [57] measurements, while the multiplication coefficients are adjusted to ensure that the modelled pedestal height matches the experimental data. Furthermore, particle diffusion is enhanced during edge localized modes (ELMs) to simulate the expulsion of heat and matter associated with ELM events. In our analysis, this is achieved using a continuous ELM model, where nominal values of density and temperature at the top of the pedestal are prescribed.

Somewhat improved approach would be if one could model SOL physics and edge sources using the EDGE2D/COCONUT workflow. However, this approach is not used in the present analysis for the following reasons:

- Complexity of Setup and Processing: The process of setting up EDGE2D/COCONUT, running the codes, and processing the results is quite complex. Given that the primary goal of this study is to assess whether simplified transport models reasonably predict the behaviour of real time D/T ratio controllers, it was determined that the benefits of using EDGE2D/COCONUT for obtaining consistent gas injection sources would be minimal in comparison to the effort involved.
- Suitability for RT Control Schemes: The complexity of these calculations makes them unsuitable for RT control schemes, which require much quicker computations. One of the main goals of the analysis is to develop a practical approach that can be implemented in RT control systems, which is why a more straightforward method using FRANTIC is employed.

In this analysis, FRANTIC is used to model gas injection. FRANTIC works in 1D geometry with radial extent from separatrix inward, not including SOL, and assumes that the gas injection is poloidally equally distributed, which simplifies the modelling. As mentioned earlier, the gas injection rates provided to FRANTIC, figures 2(*b*) and (*c*), are lower, 20%–40%, than the measured D and T gas puff rates.

3. Experimental setup

3.1. Diagnostics

Experimental data from standard JET diagnostics and recommended signals were used in the analysis. Electron density and temperature profiles were obtained from the high resolution TS diagnostics [57]. Radiated power was measured by bolometric diagnostics [58], while the effective charge state of the plasma, Z_{eff}, was assessed by means of Bremsstrahlung measurements with visible spectroscopy. The diagnostic employs both vertical and horizontal lines of sight, each passing through the plasma centre. The measured Z_{eff} is a line-averaged quantity, typically obtained from the horizontal line when localised stray-light contamination of the

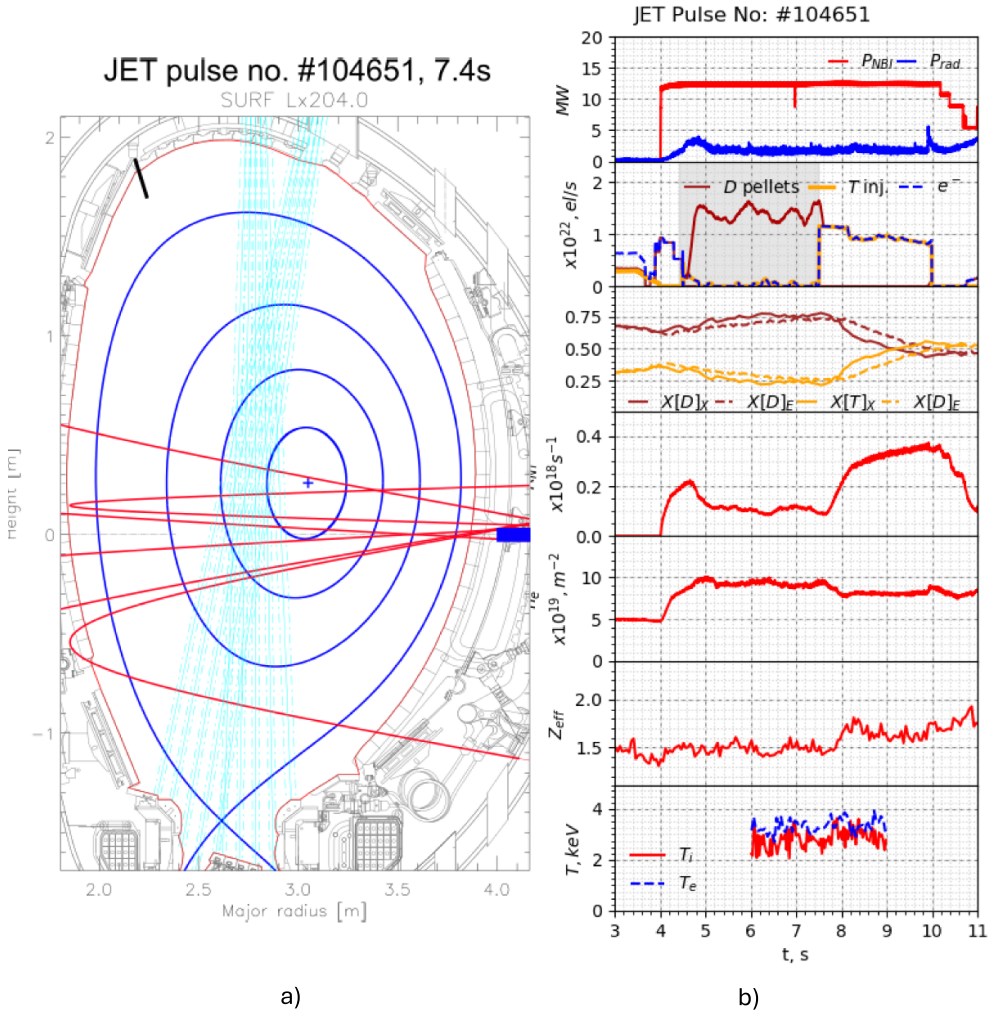

Figure 3. (*a*) Plasma cross-section of 1.4 MA/1.7 T JET pulse #104651 at 7.4 s. NBI injectors 1–6 used in this experiment are shown in red, while the pellet VHFS injection line is indicated in black. The LOS of HRS diagnostic providing the data for D/T ratio is shown in cyan. Gas injection modules used in this study are located at the LFS midplane, approximate location is shown by a blue rectangle. Time traces of investigated 1.4 MA/1.7 T JET pulse #104649 in which D/T ratio was varied by means of D/T gas injection are shown in (*b*). From top to bottom shown are traces of applied NBI power (red), P_{NBI}, and radiated power (blue), P_{rad}; pellet source of D (brown) and gas injection rates for T (orange) and electrons (blue). The time interval in which D pellets were injected is shown by greyed area. Measured D/T ratio by HRS is given on third graph by X[D]$_X$ (red solid line) and X[T]$_X$ (orange solid line), while exhaust measurements X[D]$_E$ and X[T]$_E$ are shown by dashed lines. Neutron yield, R_{NT}, line integrated electron density along the central vertical line, $\bar{n}_e$, effective charge, Z_{eff}, core electron temperatures (blue), T_e, and ion (red), T_i, temperatures are provided as well. (*c*) Electron density and temperature and ion temperature profiles for two time slices of #104651 during D pellets phase at $t = 7.42$ s (red) and T-rich phase at $t = 8.52$ s (blue).

vertical line is suspected. Neutron production counts, R_{NT}, were taken from the available neutron yield monitors [59, 60]. Ion temperature T_i for the investigated pulses is obtained from the Charge eXchange (CX) recombination spectroscopy diagnostic [61].

In general JET is equipped with two diagnostics to measure the concentration of the Hydrogen isotopes: high resolution spectroscopy (HRS) data [62–64] and mass spectrometer in the exhaust line [65]. The HRS diagnostic Line-Of- Sight (LOS) are shown in figure 3(*a*). The diagnostic provides the ratio of H, D and T neutrals to total amount of hydrogenic species as weighted average along diagnostic LOSs covering a particular section in the SOL near the X point, noted in general by r_X. These measurements are typically represented by signals of the form: $n_D(t,r_X)/(n_H(t,r_X) + n_D(t,r_X) + n_T(t,r_X))$. The measurement includes both hydrogenic neutrals from gas injection and sources due to recycling. Assuming negligible H, $n_H \approx 0$, which holds for all experiments discussed here, the following notifications $X[D]_X = n_D(t,r_X)/(n_D(t,r_X) + n_T(t,r_X))$ and $X[T]_X = n_T(t,r_X)/(n_D(t,r_X) + n_T(t,r_X))$ are adopted to distinguish between HRS measured and calculated D/T ratios. The volume averaged D/T ratios, derived from calculations, will be noted by $<X[D]> = <n_D>/< n_D + n_T>$, $<X[T]> = <n_T>/< n_D + n_T >$. Here, the angle brackets notation (e.g. $<>$) indicate that these ratios are volume-averaged quantities, highlighting the distinction between the measurements and the averaged values used in the analysis. Similarly, the notations $X[D]_E$ and $X[T]_E$ will be used for the data obtained from the mass spectrometer at the exhaust. Due to the difference in locations where measurements are

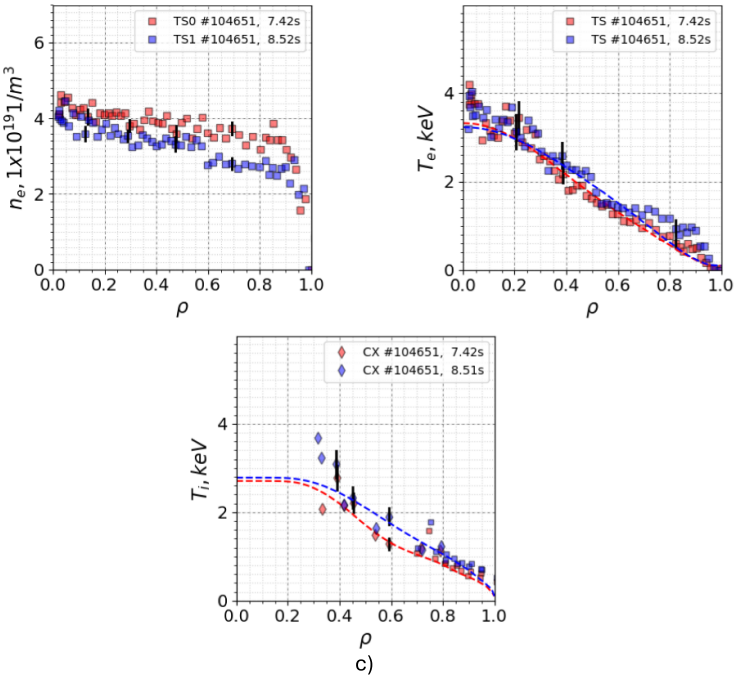

Figure 3. (Continued.)

performed, the two diagnostics discussed here, HRS and mass spectrometer in the exhaust line, are in general incompatible. Specifically, the mass spectrometer provides data from the exhaust, which, in the best-case scenario, is time-delayed relative to the actual mixture content in the plasma. For this reason, RT system in JET relies on HRS data, as it provides more realistic and timely measurements of the plasma composition compared to the mass spectrometer.

The LOS of HRS diagnostic is shown in figure 3(*a*) by cyan lines for 1.4 MA/1.7 T JET pulse #104651 at 7.4 s. In red shown are the lines of NBI injected beams, which provide central particle source. Gas injection in JET can be carried out by using various gas injection modules, with D and T injection being separated as dedicated modules are used for T injection. In our studies both D and T were injected from modules situated at the midplane on the low field side, figure 3(*a*). The amount of injected gas is calibrated [66] to ensure accurate fuelling. Additionally, the pellet injection line, which launches D pellets on the Vertical High Field Side (VHFS), is also shown in figure 3(*a*).

To assess the capability of the modelling tools used in this study, the predicted data are validated against the measurements. This validation is typically straightforward for electron densities and temperatures. However, in our studies, we model n_D and n_T, which do not directly translate into electron density. As long as the composition and impurities are modelled accurately, it can be argued that electron density can be used to validate our predictions. Additionally, as discussed in the introduction, neutron rates are highly sensitive to the D/T ratio, so these measurements can also serve to further validate the analysis.

In cases where the model output does not directly correspond to the measured data, a synthetic diagnostic can be constructed from the model. This synthetic diagnostic would correspond to a particular measurement by generating data that mirrors the diagnostic in question. For example, if SOL physics can be modelled in a 2D geometry to track the D/T isotopes transport and their recycling into the divertor region, one could perform line averaging along the HRS LOS for D/T neutral fluxes, which would then correspond to the measured data from the HRS diagnostic. Matching the data between this synthetic diagnostic and the HRS measurements could provide an indication of the quality of the modelling. Unfortunately, this approach was not feasible in our studies. 2D modelling of the SOL is complex and requires additional data, making it difficult to apply. The use of simpler codes, such as the 1D FRANTIC code to model neutral fluxes, further limits the possibility of creating a synthetic diagnostic for comparison with HRS data.

3.2. JET DTE pulses

A series of dedicated pulses were developed and conducted on JET during the DTE3 campaign, in which the D/T ratio controller was tested under fully operational conditions [7–9]. The details of these pulses, including the requested and achieved D/T ratios, are provided in table 1, along with the quantities that influence particle transport. For the pulses of interest, #104649 and #104651, the data is presented for two distinct time intervals: the first interval, during the phase of reaching D-rich plasma, while the second at the end of the phase, when a D/T ratio of 0.4/0.6 was requested. In all cases of interest, $a/L_{ne} \ll a/L_{Ti}$, meaning that particle transport and energy transport are primarily dominated by ITG turbulence. This indicates that the transport processes are more sensitive to ion temperature variations than

Table 1. Details of D/T ratio control pulses. Requested and achieved D/T ratios during early D rich and late D/T equilibration phases of the pulses are shown. T_i/T_e, density and normalised ion temperature gradient lengths and effective collisionallity ν_{eff} [67] at $\rho = 0.5$ are listed as well. Note that the a/L ratios are derived from JETTO runs. This means that a/L_{ne} is reliable only when the modelled n_e closely matches the measured data. The a/L_{Te} values are relatively accurate, as T_e is fitted to experimental data, whereas a/L_{Ti} is less precise due to the coarse mesh in T_i measurements, see figure 4(*b*).

pulse	Phase	D/T target and ***achieved ratio as measured by HRS*** at time t[s]	D/T RT control sources	T_i/T_e, a/L_{ne}, a/L_{pe}, a/L_{Te}, a/L_{Ti}, ν_{eff} at $\rho = 0.5$ at time t[s]
#104648	Phase 1, 4.5–7.5 s	D/T ≈ 0.7/0.3 ***D/T ≈ 0.75/0.25, at 7.45 s***	D by gas injection; T by gas injection	
	Phase 2, 7.5–10 s	D/T ≈ 0.4/0.6 ***D/T ≈ 0.5/0.5, at 10 s***	D by gas injection; T by gas injection	
#104649	Phase 1, 4.5–7.5 s	D/T ≈ 0.7/0.3 ***D/T ≈ 0.8/0.2, at 7.45 s***	D by gas injection; T by gas injection	$T_i/T_e \approx 0.90$, $a/L_{ne} \approx 0.52$, $a/L_{pe} \approx 3.04$, $a/L_{Te} \approx 2.53$, $a/L_{Ti} \approx 1.20$ $\nu_{eff} \approx 1.5$ at 7.43 s (from JETTO run)
	Phase 2, 7.5–10 s	D/T ≈ 0.4/0.6 ***D/T ≈ 0.47/0.53, at 10 s***		$T_i/T_e \approx 1.02$, $a/L_{ne} \approx 0.45$, $a/L_{pe} \approx 2.86$, $a/L_{Te} \approx 2.42$, $a/L_{Ti} \approx 2.14$ $\nu_{eff} \approx 0.95$ at 8.88 s (from JETTO run)
#104650	Phase 1, 4.5–7.5 s	D/T ≈ 0.7/0.3 ***D/T ≈ 0.75/0.25, at 7.45 s***	D by pellets;	
	Phase 2, 7.5–10 s	D/T ≈ 0.4/0.6 ***D/T ≈ 0.44/0.56, at 10 s***	T by gas injection	
#104651	Phase 1, 4.5–7.5 s	D/T ≈ 0.7/0.3 ***D/T ≈ 0.77/0.23, at 7.45 s***	D by pellets;	$T_i/T_e \approx 1.00$, $a/L_{ne} \approx 0.29$, $a/L_{pe} \approx 2.76$, $a/L_{Te} \approx 2.47$, $a/L_{Ti} \approx 2.79$ $\nu_{eff} \approx 1.5$ at 7.43 s (from JETTO run)
	Phase 2, 7.5–10 s	D/T ≈ 0.4/0.6 ***D/T ≈ 0.44/0.56, at 10 s***	T by gas injection	$T_i/T_e \approx 1.09$, $a/L_{ne} \approx 0.34$, $a/L_{pe} \approx 2.41$, $a/L_{Te} \approx 2.07$, $a/L_{Ti} \approx 1.71$ $\nu_{eff} \approx 1.0$ at 8.50 s (from JETTO run)

to electron density gradients, and ITG turbulence plays a key role in governing the overall transport behaviour in these scenarios.

In these 1.4 MA/1.7 T pulses heated with $P_{NBI} \approx 12$ MW of D NBI power the plasma was initially fuelled with D neutral gas either by gas injection, figure 4(*a*), or pellets, figure 3(*b*), so that D/T ratio has been forced to increase to about D/T ≈ 0.8/0.2. This D rich plasma was achieved via RT control of D and T gas in response to the requested reference values during the initial period 4.5–7.5 s of high performance H-mode phase, see table 1. This is shown in figure 4(*a*) for #104649 with D gas injection rates of $\Gamma_{D,inj} \approx 1.3 \times 10^{22}$ 1/s (brown line in second graph) and in figure 3(*b*) for #104651 where pellets (grey area in second graph) were injected from about 4.5 s until 7.5 s. In this case small pacing pellets with radius of 1 mm and length of 1.7 mm were injected with rate of about 40 pellets per second. The RT controller was then programmed to adjust the D/T ratio to a more favourable mix, such as around 0.4/0.6. The requested and achieved D/T ratios during these experiments are provided again in table 1. Signals from the HRS on D and T ion ratios, $X[D]_X$ and $X[T]_X$, were used as inputs for the RT controller in the described RT algorithm [7]. Time traces of D/T ratio for the two pulses, one fuelled with D gas injection and the other by D pellets, are shown on third graph in figures 4(*a*) and 3(*b*). To achieve the requested equipartition of the D/T ratio, the RT algorithm acted on D source by stopping it and enabling the T source. Specifically, in pulse #104649 (gas injection) and pulse #104651 (pellets), the D injection was stopped at 7.5 s, and shortly after, T gas injection began at a rate of approximately $\Gamma_{T,inj} \approx 1.1 \times 10^{22}$ 1 s^{-1}. As a result of this adjustment, the D/T ratio reached approximately 0.5/0.5, responding to the RT control request with a delay of about 1–1.5 s. This change in the D/T ratio led to an improvement in fusion performance, as indicated by the R_{NT} time traces shown in figures 3(*b*) and 4(*a*), while electron density, temperatures, and Z_{eff} remained unchanged.

The time constants, which represent the rate of exponential changes in $X[D]_X$ and $X[T]_X$ signals, as well as the R_{NT} signals, are an important aspect of these studies and are briefly discussed here. In pulse #104649, where gas-injected D is used, the time constants for the D/T ratio signals, $X[D]_X$ and $X[T]_X$, are approximately equal to the time constant of the neutron yield, R_{NT}, with all three being between 0.94 s and 0.96 s, as shown in figure 4(*a*). In the pellet-fuelled pulse #104651, the time constants for $X[D]_X$ and $X[T]_X$ are similar, around 0.89 s. However, the fusion yield changes on a much quicker timescale, with a time constant of 0.51 s, as shown in

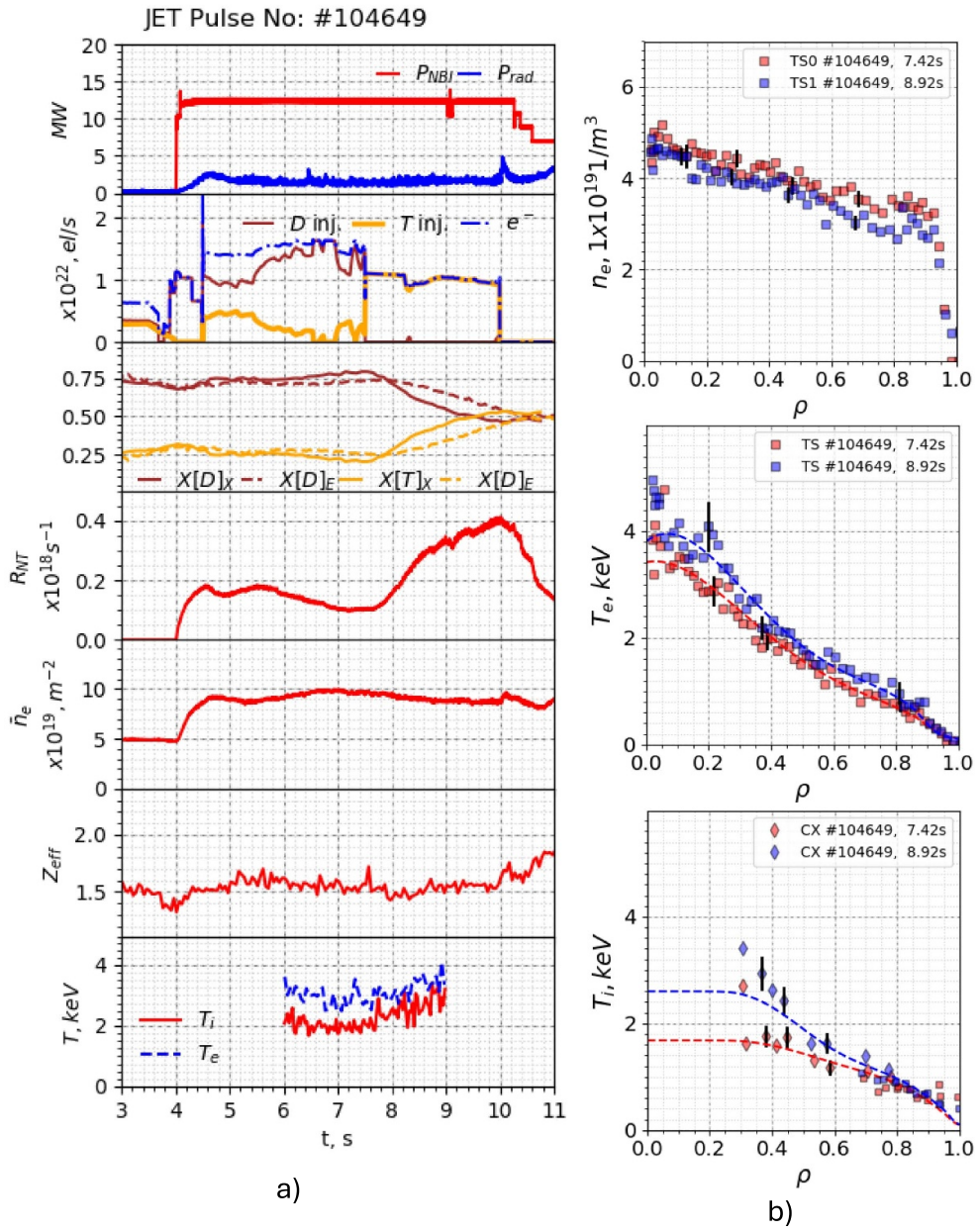

Figure 4. (*a*) Time traces of investigated 1.4 MA/1.7 T JET pulse #104649 in which D/T ratio was varied by means of D/T gas injection. From top to bottom shown are traces of applied NBI power (red), P_{NBI}, and radiated power (blue), P_{rad}, gas injection rates for D (red), T (orange) and electrons (blue), measured D/T ratio, $\mathrm{X[D]_X}$ in red and $\mathrm{X[T]_X}$ in orange, neutron yield, $\mathrm{R_{NT}}$, line integrated electron density, $\bar{n}_{\mathrm{e}}$, effective charge, Z_{eff}, core electron (blue), T_{e}, and ion (red), T_{i}, temperatures. (*b*) electron density and temperature and ion temperature profiles for #104649 at $t = 7.42$ s (red) and $t = 8.92$ s (blue).

figure 3(*b*). This shows that the fusion yield responds faster than the D/T ratio signals in the pellet-fuelled pulse.

The electron density, electron temperature, and ion temperature profiles for two time slices—at the end of the D-rich phase, at 7.42 s, and during the equipartition phase with a D/T $\sim$ 0.5/0.5 ratio, at 8.92 s, are shown in figure 4(*b*).

While there are some changes in the profiles, particularly in ion temperature, T_{i}, the pedestal stored energy only changes by about 11%. This supports the approach used in the study, where the pedestal is modelled independently from the core, with the neglect of core to edge coupling being a reasonable approximation for the given scenarios.

4. Results from the analysis

In the following section the results from interpretative TRANSP runs and predictive JETTO analysis are presented and validated versus the experimental data: total neutrons

count, R_{NT}, T concentration, $X[T]_X$ signal from HRS, and electron density profile evolution, $n_e(t,\rho)$.

4.1. Interpretative TRANSP simulations

TRANSP was run fully interpretatively, incorporating electron density and temperature from TS measurements, while ion temperature and rotation profiles were obtained from CX diagnostics. The impurity used in CX measurements is Ne. The plasma composition was computed using a prescribed workflow in which the densities of D and T ions were constrained to maintain quasi-neutrality and align with Z_{eff} measurements. The D/T ratio was kept constant along plasma radius and inferred from HRS measurements, which provide $X[D]_X$ and $X[T]_X$, representing the D/T mixture at the SOL.

The plasma composition was assumed to consist of a time- and space-varying D/T mixture along with two impurities, Be and Ni. The electron density profile, $n_e(t,\rho)$, was mapped using pressure-constrained EFIT [68] reconstruction, while Z_{eff} measurements provided only the time evolution of Z_{eff} with a constant profile. This approach determines the densities of hydrogenic species and one impurity (Ni), while for Be, a fixed ratio of $n_{Be}/n_e = 0.01$ was assumed, based on recent JET studies [69], which suggest this is a reasonable assumption.

The hydrogenic density was further divided into n_D and n_T densities by imposing the measured $X[D]_X$ (or equivalently $X[T]_X$) constraint. A key feature of this approach is that it constrains both n_D and n_T profiles evolution to align with n_e, Z_{eff}, $X[D]_X$ and beam source evolution. However, this method does not account for particle transport and cannot predict the evolution of n_D and n_T as gas injection sources change. Its sole purpose is to validate prescribed n_D and n_T profiles against experimental data for R_{NT}.

A notable limitation of this approach is that it relies on the measured $X[D]_X$ ratio from the divertor SOL region near the X-point, as shown in figure 3(*a*). Since this measurement does not represent the entire plasma volume, discrepancies arise because the actual X[D] distribution within the plasma differs from $X[D]_X$. As a result, using $X[D]_X$ introduces potential errors in both the analysis and the RT control scheme.

The results of the TRANSP simulations are summarised in figure 5. Despite the simplified approach used for modelling the D/T mixture in TRANSP, figure 5(*a*) demonstrates that the calculated neutron yield closely matches the experimental

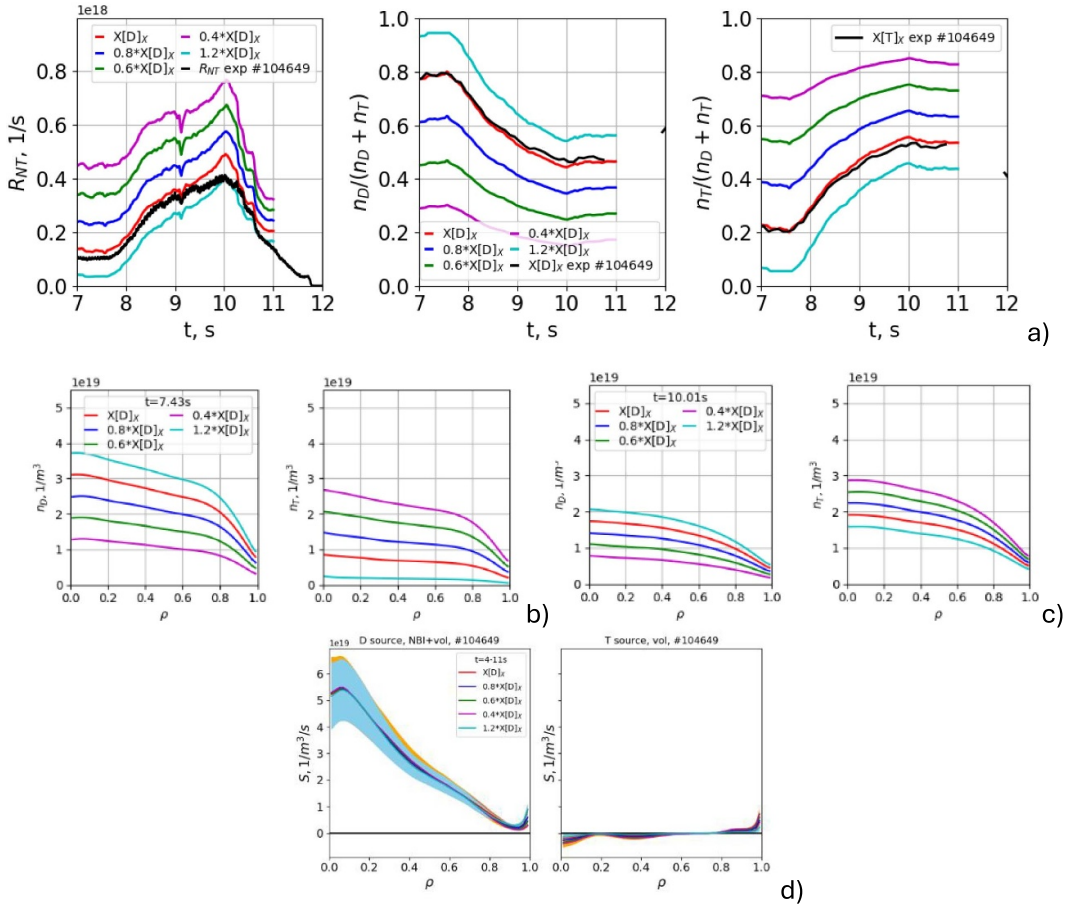

Figure 5. (*a*) Results from TRANSP simulations of #104649 for measured R_{NT}, $X[D]_X$ and $X[T]_X$ (black) and calculated R_{NT} and calculated <X[D]> and <X[T]> for the cases when real $X[D]_X$ was used to deduce D/T ratio (red) and for cases with scaled $X[D]_X$ ratio: 0.8^* $X[D]_X$ (blue), 0.6^* $X[D]_X$ (green), 0.4^* $X[D]_X$ (magenta) and 1.2^* $X[D]_X$ (cyan). Corresponding n_D and n_T profiles at 7.43 s are shown in (*b*) and at 10 s in (*c*); (*d*) calculated volume sources of D and T due to NBI and halo in time interval 4–11 s.

data. When the D/T ratio is taken from HRS measurements, the calculated R_{NT} (red line) closely follows the measured neutron count, accurately reproducing the transient phase. In contrast, using a scaled $X[D]_X$ leads to significant deviations from the measured R_{NT}, as seen in figure 5(*a*). This suggests that while HRS measurements are taken from the SOL near the X-point, their quality is sufficiently high to be considered for a D/T ratio control system, i.e. $X[D]_X \approx <X[D]>$, making HRS data a reasonable proxy for the D/T ratio within the plasma. The observation that $X[D]_X \approx <X[D]>$ is consistent with ion mixing theory [38, 39]

Figures 5(*b*) and (*c*) show the evolution of n_D and n_T. The D ion density, n_D, includes NBI D ion source which is consistent with the workflow used in these TRANSP simulations. Both profiles follow the evolution of the electron density n_e, as seen at 7.43 s (compare figures 4(*b*) and 5(*b*)). As the plasma parameters evolve, n_D and n_T profiles continue to mirror the evolution of n_e maintaining their initial shape.

A key question is whether this workflow can be used to develop a RT control scheme for D/T mixture control. For feasibility, RT signals for n_e, $X[D]_X$ (either $X[D]_X$ or $\langle X[D] \rangle$), Z_{eff}, and, if significant, the beam source, would be required. In implementing such a scheme, a realistic assumption about impurities should be made. In this study, we assume fully ionized Be and Ni with $n_{Be}/n_e = 0.01$, a reasonable assumption for future thermonuclear machines where impurity sources and transport are well-characterized, as was the case during the late JET DTE experiments. The only remaining uncertainty is the beam source. However, figure 5(*d*) shows that in a given scenario, variations in the beam source are minimal over a broad range of D/T ratios.

The discussion above strongly indicates that, based on TRANSP modelling, a simplified model can be developed and implemented in RT D/T ratio control schemes. By providing an RT control tool with inputs from n_e, X[D], Z_{eff}, and an initial estimate of the NBI source, a control scheme using gas injection actuators—based on simplified quasi-neutrality and Z_{eff} calculations—should perform satisfactorily, as supported by the results presented here.

4.2. JETTO simulations with predictive particle transport: comparison to experiment

JETTO was run predictively for n_D and n_T densities, while the electron and ion temperatures evolution were fixed to the corresponding measured values. The particle diffusion coefficient, D_D and D_T, which govern conductive particle transport, and the inward pinch terms, V_D and V_T, which represent convective transport, were varied. As discussed in the previous section, BgB model [31] was used to calculate electron and ion heat diffusivities according to equations (1) to (3), while ions diffusivities, D_D and D_T, were derived according to equation (4). A summary of the key settings in performed JETTO runs is provided in table 2.

4.2.1. Fuelling by gas injection only. Results from JETTO modelling of JET pulse #104649 which was fuelled by gas injection of D and T are shown in figure 6.

In this workflow, initial simulations were conducted to fine-tune the parameters of the H-mode pedestal barrier and the FRANTIC gas injection rates. The latter provide particle sources, which are localized in the pedestal region, figures 2(*b*) and (*c*). The pedestal width was determined from measurements, while the sources and transport coefficients within the pedestal were adjusted to match the observed pedestal height. Once the pedestal and gas injection sources were established, a multidimensional parameter scan was performed across the A_1, A_2, and α_i parametric space, see equations (4) and (5). This scan was facilitated by a newly developed API in JETTO [70].

The scans were evaluated by minimizing the chi-square difference between the modelled and measured electron density,

Table 2. Details of JETTO simulations.

	Equilibrium	T_e, T_i	n_D, n_T	Neutrals	Impurities	Rotation
Mode Evolving	Evolving with prescribed boundary	Prescribed	Predictive	Predictive (only profile shape)	Predictive	Prescribed
Codes JETTO	ESCO	From measurements	BgB, (QuaLiKiz)	FRANTIC	SANCO, calculated Zeff	From measurements
	Boundary from EFTP	TS and CX data			Be, Ni, W	CX data

Heating/fuelling	Fusion	Radiation	n_D, n_T sources	ETB	MHD
Predictive PENCIL	Predictive JETTO	Prescribed From measurements	Predictive FRANTIC, HPI2 (cont model), PENCIL	Prescribed JETTO, fixed barrier width	Prescribed JETTO, ELM continuous TOB model
		Bolometry data			

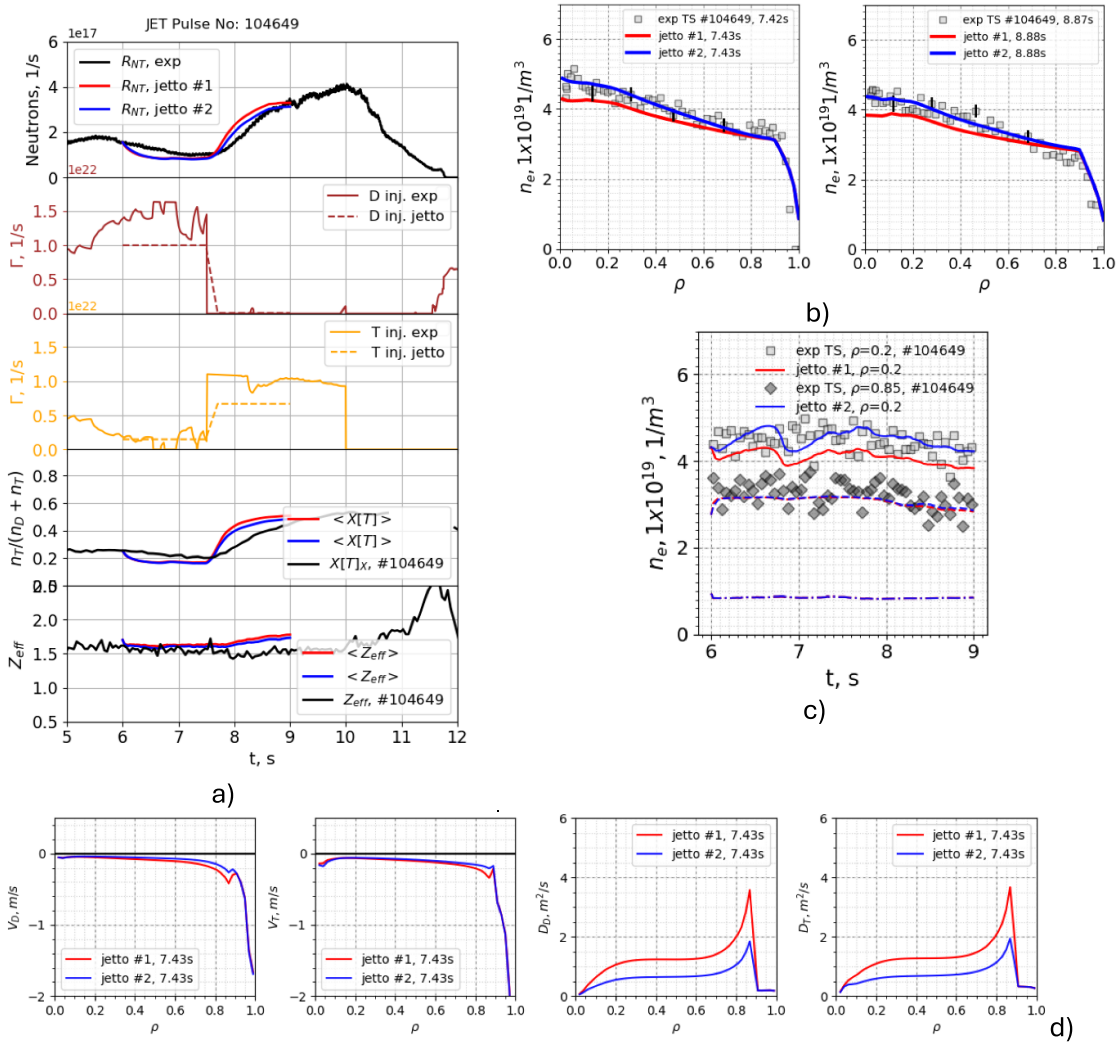

Figure 6. Results of two JETTO simulations of #104649 with Bohm-gyroBohm model and particle diffusion coefficients $A_1 = 8, A_2 = 4$ (jetto #1 red) and $A_1 = 4, A_2 = 2$ (jetto #2 blue). Time traces of R_{NT}, D and T gas injection rates, measured X[T]$_X$ (black) and calculated <X[T]> (red and blue) and Z_{eff} are shown from top to bottom in (*a*). Calculated and measured n_e for two time slices, 7.42 s and 8.87 s, are shown in (*b*) while measured and calculated n_e time traces in the core, for $\rho = 0.2$ (squares and solid red and blue lines), and at the pedestal, at $\rho = 0.85$ (diamonds and dashed red and blue lines), are plotted in (*c*) together with JETTO boundary condition at $\rho = 1$ (dash-dotted lines). Transport coefficients for the two cases are shown at 7.42 s in (*d*) from left to right V_D, V_T for D and T pinch velocities and D_D, D_T for D and T particle diffusivities.

n_e, and neutron yield, R_{NT}. Figure 6 presents the results for two of the best-fitting parameter sets: $A_1 = 8, A_2 = 4, \alpha_i^{inw} = 0.05$ and $A_1 = 4, A_2 = 2, \alpha_i^{inw} = 0.05$. A strong agreement between the modelled and measured n_e profile evolution and R_{NT} time traces was achieved when the FRANTIC gas injection rates were slightly reduced, figure 6(*a*) second and third graphs. In the initial D-rich phase, the FRANTIC D gas injection rate was set to $\Gamma_{D,jetto} \approx 1 \times 10^{22}$ 1 s^{-1}, approximately 40% lower than the experimental injection rate, $\Gamma_{D,inj}$. Similarly, in the T-rich phase, the FRANTIC T gas injection rate $\Gamma_{T,jetto}$ needed to be reduced by about 30% compared to experimental values, $\Gamma_{T,inj}$, to match the steady-state $\langle X[T] \rangle$.

Discrepancies in the D/T ratio, figure 6(*a*), between the HRS measurement, X[T]$_X$, and the JETTO result, $\langle X[T] \rangle$, primarily arise in their rate of increase. However, after the transient ramp-up of X[T]$_X$, the steady-state values are consistent, with <X[T]> $\approx$ X[T]$_X$ $\approx$ 0.2 at 7.45 s and <X[T]> $\approx$ X[T]$_X$ $\approx$ 0.5 at 9 s. The difference in time evolution can be attributed to the measurement locations: HRS provides X[T]$_X$, representing the T concentration in the divertor SOL region, while JETTO calculates $\langle X[T] \rangle$, an averaged value over the plasma. More detailed explanations are provided in the next paragraph.

In the experiments presented, T gas was injected from the midplane LFS, figure 3(*a*). Assuming high T injection efficiency (i.e. high ratio of $n_{T,sep}/\Gamma_{T,inj}$) and negligible leakage of injected T gas into the divertor region, the main contributor to the measured X[T]$_X$ in HRS is expected to be from T recycling. This recycling process occurs on a slow timescale, as it involves the penetration of injected T into the core. In contrast,

JETTO assumes poloidally uniform gas injection, leading to a faster evolution of ⟨X[T]⟩ compared to the experimental $X[T]_X$, where the effects of penetration and recycling have more significant impact. To incorporate recycling effects in the simulations, recycling coefficients of 10% for both D and T were applied in FRANTIC, consistent with modelling studies for ITER-like wall conditions [44].

Theoretical studies [38] suggest that for H/D mixtures in an ITG-dominated turbulence regime, the diffusion coefficients for D and H ions range between 1.2–2.6 $m^2\ s^{-1}$ when switching from a D to an H source, table 5 in [38]. For the case with $A_1 = 8$, $A_2 = 4$, the diffusivities at $\rho = 0.5$ were $D_D \approx D_T \approx 1.2\ m^2\ s^{-1}$, figure 6(*d*), which aligns with these theoretical predictions, considering that the present experiment involves a D/T mixture rather than H/D. While [38] predicts larger convective velocities, the combination of pure convection and thermo-diffusion—both of similar magnitude but opposite in sign—results in a small net convection term, consistent with the values shown in figure 6(*d*).

4.2.2. Fuelling by gas injection and pellets. The case in which initial D fuelling was performed using pellets, specifically JET pulse #104651, is discussed here, with JETTO simulation results presented in figure 7. Pellets were very successfully used in previous JET campaigns to control D/H mixture [71]. Two pellet models were employed in this study: HPI2 and the continuous model.

The HPI2 model is a first-principles physics model that accounts for pellet ablation and deposition. However, running JETTO with HPI2 is computationally expensive and

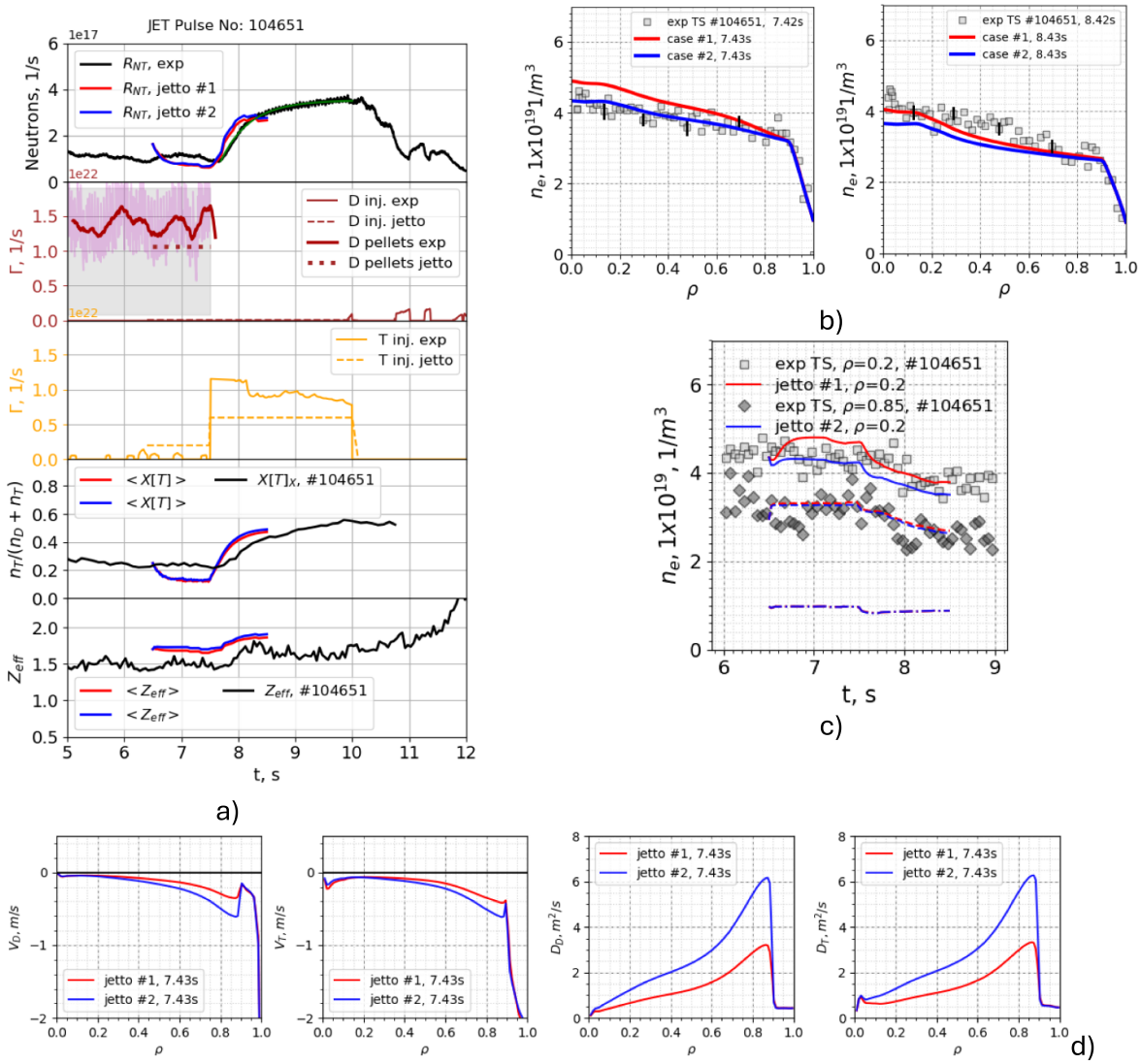

Figure 7. Results of two JETTO simulations of #104651 with Bohm-gyroBohm model and particle diffusion coefficients $A_1 = 4$, $A_2 = 2$ (jetto #1 red) and $A_1 = 8$, $A_2 = 4$ (jetto #2 blue). Time traces of R_{NT}, D and T gas injection rates, measured $X[T]_X$ (black) and calculated <X[T]> (red and blue) and Z_{eff} are shown from top to bottom in (*a*). Calculated and measured n_e for two time slices, 7.43 s and 8.43 s, are shown in (*b*) while measured and calculated n_e time traces in the core, for $\rho = 0.2$ (squares and solid red and blue lines), and at the pedestal, at $\rho = 0.85$ (diamonds and dashed red and blue lines), are plotted in (*c*) together with JETTO boundary condition at $\rho = 1$ (dash-dotted lines). Transport coefficients for the two cases are shown at 7.43 s in (*d*) from left to right V_D, V_T for D and T pinch velocities and D_D, D_T for D and T particle diffusivities.

slow, particularly in scenarios requiring parameter scans. In contrast, the continuous pellet model assumes a prescribed Gaussian pellet deposition profile in toroidal ρ, making it significantly faster and more practical for performing large-scale scans. To balance accuracy and efficiency, an initial short-timescale run using the HPI2 model was conducted to estimate realistic pellet ablation and deposition, i.e. particle source. Once the real pellet deposition was determined, a Gaussian fit was applied, figure 2(*c*), allowing the continuous model to be used for extended simulations.

The results from JETTO modelling of JET pulse #104651, where D pellets were used for initial fuelling and T gas injection was applied in the second phase, are shown in figure 7. Two parameter sets for particle diffusion and pinch velocity coefficients were tested: $A_1 = 4$, $A_2 = 2$, $\alpha_i^{\mathrm{inw}} = 0.05$ and $A_1 = 8$, $A_2 = 4$, $\alpha_i^{\mathrm{inw}} = 0.05$.

Similarly to pulse #104649, figure 6, in the pellet-fuelled case, the T injection rates in FRANTIC had to be reduced during the D/T ratio equipartition phase, i.e. after 7.5 s. Interestingly, we found that a small amount of T injection or recycling needed to be assumed during the initial phase when a D-rich plasma was being established, figure 7(*a*), third graph, before 7.5 s. The small amount of tritium likely originates from legacy deposits on tiles, left from past discharges, and it is now released through recycling process. Without this additional T ion source, the D/T ratio in our simulations would rapidly evolve toward nearly 1.0/0.0. However, even with the assumed small T injection, the simulations remained inconsistent with the measured D/T ratio of approximately 0.8/0.2 at 7.5 s. One possible explanation for this discrepancy is that the real D pellet fuelling was overestimated in the simulations and somewhat in the experimentally assessed rates, figure 7(*a*). Although both the JETTO model and the experimentally assessed rates consistently indicate rates of about 1.1–1.3 $\times$ 10^{22} 1 s^{-1} it is possible that not all pellets produced and detected in the feeding line were successfully delivered to the plasma. The latter is plausible because the pellet monitor cannot distinguish between intact pellets and gas produced by pellets ablation or pellets destroyed in the flight line, which can readily lead to overestimation.

Despite this inconsistency in the modelled D/T ratio before 7.5 s, the model predicts the n_e profiles and R_{NT} evolution reasonably well. The initial D-rich phase is best reproduced for higher transport coefficients, $A_1 = 8$, $A_2 = 4$ (blue curves), while the equipartition phase after 7.5 s is better captured with lower transport coefficients, i.e. $A_1 = 4$, $A_2 = 2$ (red curves). However, in both cases, the density profiles at mid-radius in the second phase are somewhat underpredicted. The D/T ratio evolution, $\langle \mathrm{X[T]} \rangle$, is poorly matched during the initial stage and only aligns with the measured $\mathrm{X[T]_X}$ toward the end of the simulation, around 8.5 s.

4.3. JETTO simulations with predictive particle transport: case studies

Having demonstrated JETTO's predictive capabilities in modelling D/T ratio control experiments, the next step is to leverage the code to investigate the impact of all actuators operating across their full range. Due to various technical constraints and limited operational time, several planned experiments intended to complement the described studies were not completed. These unperformed experiments are now being explored through JETTO predictive modelling analysis, allowing for a comprehensive assessment of their expected outcomes.

4.3.1. Swapping D and T injection. JET pulse #104649 demonstrated the full capabilities of D/T ratio control through D and T gas injection. However, due to the tight experimental schedule, it was not possible to experimentally swap the D/T injection sequence and study the recovery from a T-rich plasma to a D/T ratio of approximately 0.5/0.5. Now, with the validated JETTO model, we have the opportunity to investigate this reversed scenario, where the D and T gas injections are swapped. The results of this simulation are presented in figure 8.

Interestingly, in the reverse scenario simulations, despite an initial overflow of T gas into the vessel, a T-rich plasma could not be achieved, as shown in figure 8(*a*). In contrast, with similar but reversed injection rates, a D-rich plasma was successfully achieved before 7.5 s, as seen in figure 6(*a*). The main suspected reason for this disparity appears to lie in the NBI fuelling. Despite the NBI particle source being an order of magnitude lower, figure 2, it seems to play an important role in regulating the D/T ratio in the core. With the initial conditions set to small D and large T injection, the reversed scenario quickly evolves from a D/T ratio of 0.8/0.2 to approximately 0.5/0.5. Following this, the disbalancing of gas injection—shutting down T injection and continuing D injection—further lowers the $\mathrm{X[T]_X}$ ratio.

This example clearly highlights the importance of examining future RT controllers using particle transport simulations first. This approach ensures that RT controller parameters can be optimized for better performance in regulating D/T ratios and improving overall plasma control.

4.3.2. Fuelling with T pellets. JET pulse #104651 demonstrated, for the first time, D/T ratio control through the use of pellets. However, due to hardware limitations—specifically the pellet injector's inability to produce T pellets—the experiment could not be fully explored, particularly in terms of demonstrating operations with two pellet injectors. This would be an important step for future fusion machines, which are

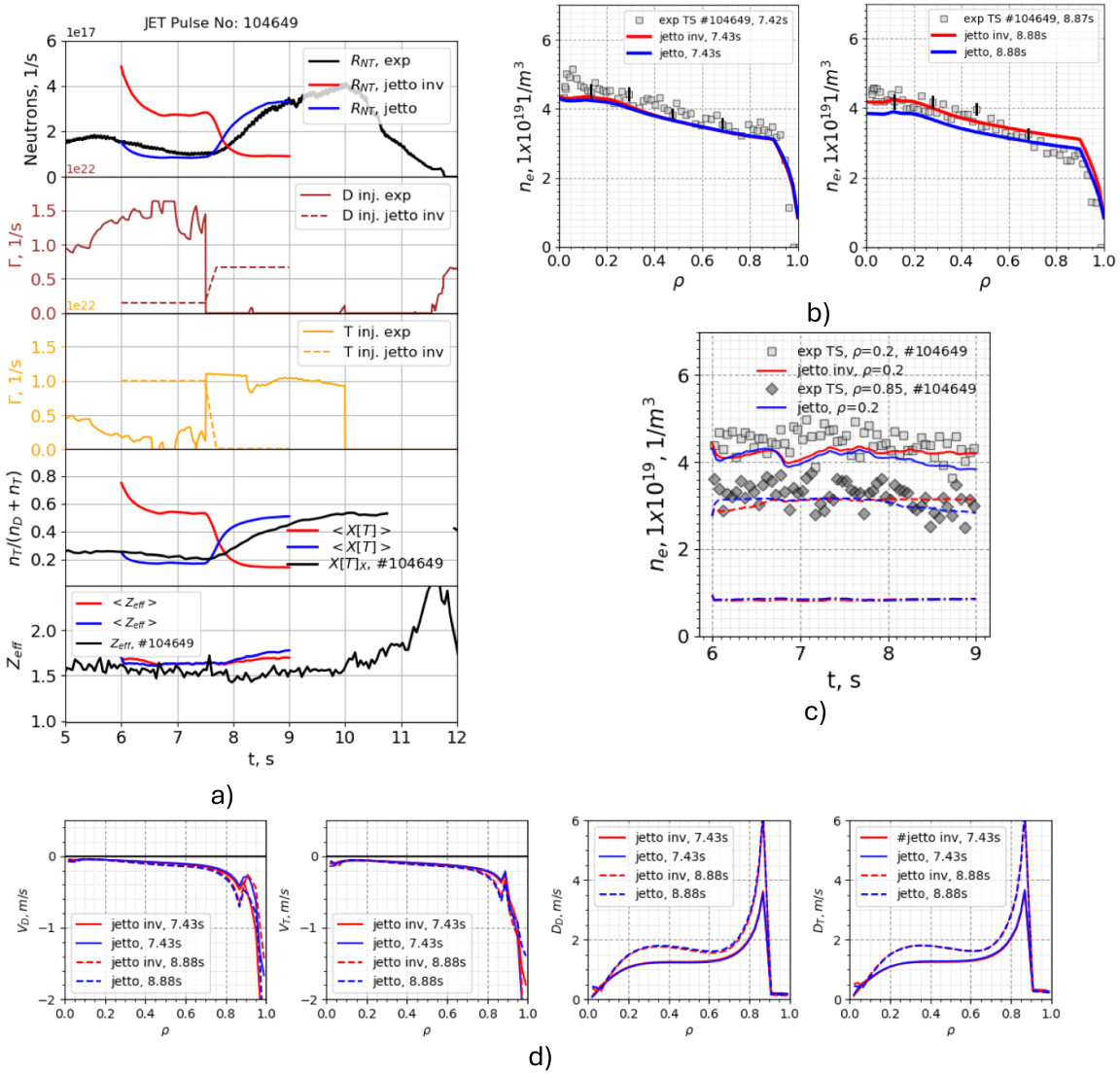

Figure 8. Results of two JETTO simulations of pulse #104649, with particle diffusion coefficients $A_1 = 8$, $A_2 = 4$, are presented for both the standard experimental sequence (labelled 'jetto' in blue) and a reversed scenario (labelled 'jetto inv' in red), where T injection was used initially to create a T-rich plasma before 7.5 s, followed by D injection to achieve a more balanced D/T ratio. The time traces of R_{NT}, D and T gas injection rates, measured $X[T]_X$ (black), and calculated $\langle X[T] \rangle$ (red and blue), along with Z_{eff}, are shown in (*a*). Calculated and measured electron densities n_e for two time slices, 7.43 s and 8.88 s, are presented in (*b*). Measured and calculated n_e time traces in the core ($\rho = 0.2$, squares and solid red/blue lines) and at the pedestal ($\rho = 0.85$, diamonds and dashed red/blue lines) are shown in (*c*). It is important to note that the reversed scenario case (red curves) represents a simulation, not an actual experiment, and thus direct comparison with measurements is not valid. The measured data in this case are provided for illustration purposes only.

planned to use pellets for both D and T injection. The case in which D/T ratio control was performed with T pellets in the initial phase followed by D injection was now investigated using JETTO simulations. The results of this analysis for the T pellets scenario are shown in figure 9.

Similar to the D pellet case shown in figure 7, the T pellet fuelling proves to be highly effective in achieving a T-rich plasma, as seen in figure 9(*a*). D/T ratios of approximately 0.3/0.7 were quickly reached despite the small D injection and NBI D fuelling. Once the T pellets were stopped and D injection was increased after 7.5 s, the initial phase quickly transitioned to a D-rich plasma.

The predicted neutron rate closely follows the $\langle X[T] \rangle$ trend, indicating consistency with expected improved fusion performance for D NBI heated T-rich plasma, as described in [6]. This demonstrates the capability of T pellet fuelling to effectively control the D/T ratio and enhance plasma performance, even with limited D injection.

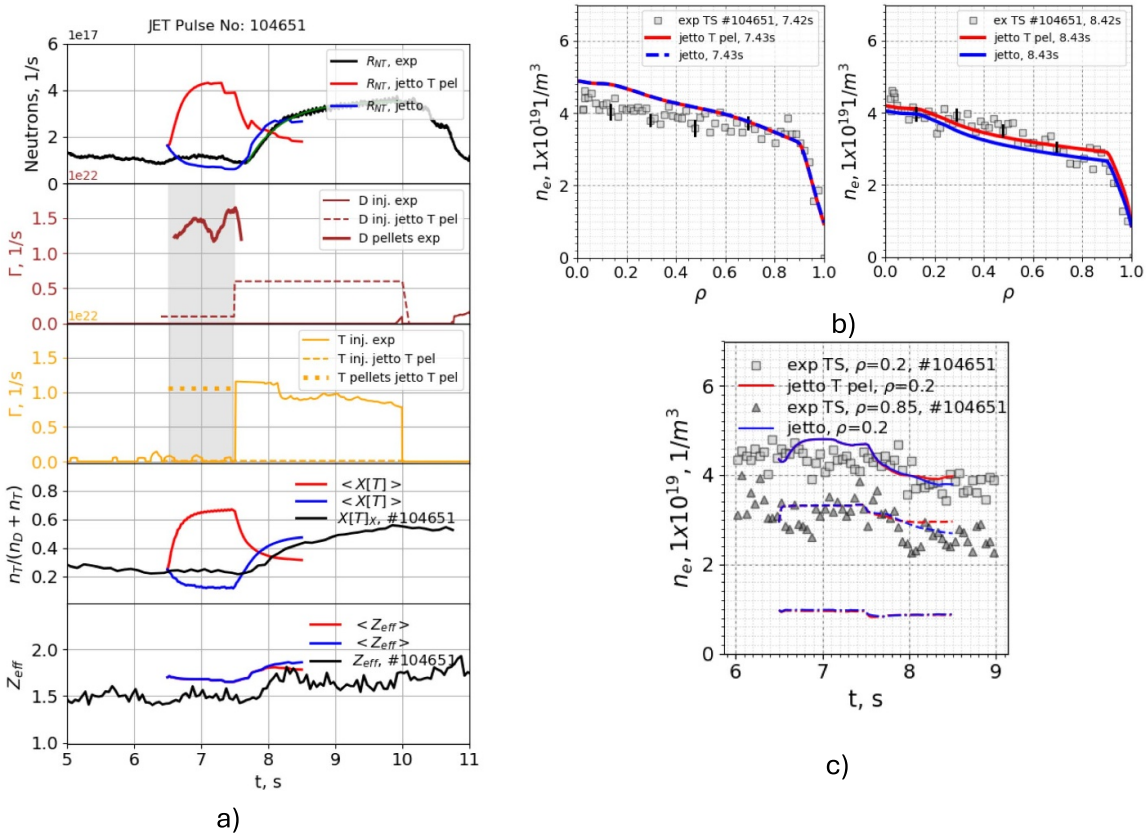

Figure 9. Results of two JETTO simulations of #104651 with particle diffusion coefficients $A_1 = 4, A_2 = 2$ (labelled 'jetto' in blue) and simulation in which T and D sources were swapped with T pellets and the beginning and D gas injection in the second phase (labelled 'jetto T pel' in red). Time traces of R_{NT}, D and T gas injection rates, measured $X[T]_X$ (black), and calculated $\langle X[T] \rangle$ (red and blue) and Z_{eff} are shown in (*a*). T pellet time window is shown by grey area in (*a*). Calculated and measured n_e for two time slices, 7.43 s and 8.43 s, are shown in (*b*) while measured and calculated ne time traces in the core, for $\rho = 0.2$ (squares and solid red and blue lines), and at the pedestal, at $\rho = 0.85$ (triangles and dashed red and blue lines), are plotted in (*c*). It is important to note that T pellet scenario case (red curves) is not a real experiment and simulations must not be directly compared to measurements. Measured data in this case is only provided for illustration.

5. Conclusions

The results presented here clearly demonstrate that simple models and assumptions regarding D and T transport and sources can be successfully adopted to predictively model the behaviour of RT controllers for D/T ratio. However, these models exhibit certain limitations that must be acknowledged—specifically, their limited accuracy in capturing the evolution of the D/T ratio during transient phases, particularly when fuelling rates undergo significant changes. It is not necessary to model the SOL and core in detail across all channels to carry out such tasks. This study shows that a simplified approach can be effective, using (i) measured T_e, T_i, (ii) not modelling the SOL physics, and (iii) simplifying particle transport assumptions. This conclusion is crucial for developing numerical tools to test future controllers.

For future RT controller development aimed at D/T ratio control, the models presented here would serve as a foundation for further improvements. For example, as demonstrated by TRANSP modelling, an RT scheme based on simple quasi-neutrality and Z_{eff} calculations could be implemented successfully. This study shows that such a scheme would work well with rough estimates of impurities and NBI particle sources.

Additionally, modelling the response of the desired output—D/T ratio in this case—across various scenarios, as demonstrated through JETTO predictive particle modelling, would be a valuable outcome from this study. For adjusting and optimizing RT controllers, this workflow could save experimental time and reduce the need for expensive computations.

In general, the proposed approach for developing and testing RT D/T controllers should be directly applicable to future conventional tokamaks, such as ITER, SPARC, and DEMO, where simplified assumptions about energy and particle transport are valid. For devices where the transport models require validation—such as STEP—applicability largely depends on the extent to which transport can be reasonably simplified. Regarding the source terms, the proposed model appears broadly applicable. The simulations presented here indicate that particle sources from pellet injection and NBI can be reliably captured by the models employed in this work. However, for gas injection sources, the simplified treatment used in the

FRANTIC code may not be adequate for devices or scenarios characterized by significantly different SOL physics.

Acknowledgment

This work has been carried out within the framework of the EUROfusion Consortium, funded by the European Union via the Euratom Research and Training Programme (Grant Agreement No 101052200—EUROfusion) and from the EPSRC [Grant Numbers EP/W006839/1]. Views and opinions expressed are however those of the author(s) only and do not necessarily reflect those of the European Union or the European Commission. Neither the European Union nor the European Commission can be held responsible for them.

The Author K. K. is greatly appreciative of the discussions with C. Angioni, M. Maslov and T. Tala regarding particle transport in mixed DT plasma.

ORCID iDs

K.K. Kirov 0000-0001-8104-4782
M. Lennholm 0000-0002-3444-3999
L. Piron 0000-0002-7928-4661
M. Baruzzo 0009-0006-7853-7280
M. van Berkel 0000-0001-6574-3823
T. Bosman 0000-0002-7922-7974
L. Ceelen 0000-0002-6574-1841
L. Garzotti 0000-0002-3796-9814
B. Kool 0000-0002-1636-7400
J. Mitchell 0000-0001-6639-4127
B. Sieglin 0000-0002-9480-4434
H. Sun 0000-0003-0880-0013

References

[1] Maggi C. *et al* 2024 *Nucl. Fusion* **64** 112012
[2] Garzotti L. *et al 2023 29th IAEA Fusion Energy Conf. (FEC 2023)* (*London, United Kingdom, 16–21 October 2023*) (available at: https://www.iaea.org/events/fec2023)
[3] Garzotti L. *et al* 2025 *Plasma Phys. Control. Fusion* **67** 075011
[4] Hobirk J. *et al* 2023 *Nucl. Fusion* **63** 112001
[5] Kappatou A. *et al* 2025 *Plasma Phys. Control. Fusion* **67** 045039
[6] Maslov M. *et al* 2023 *Nucl. Fusion* **63** 112002
[7] Lennholm M. *et al* 2025 *PRX Energy* **4** 023007
[8] Piron L. *et al* 2021 *Fusion Eng. Des.* **166** 112305
[9] Baruzzo M. *et al* 2025 *30th IAEA Fusion Energy Conf. (FEC 2025)* (*Chengdu, People's Republic of China, 13–18 October 2025*) (available at: https://www.iaea.org/events/fec2025)
[10] Valovič M. *et al* 2024 *Nucl. Fusion* **64** 076013
[11] ITER Physics Basis Editors, ITER Physics Expert Group Chairs and Co-Chairs and ITER Joint Central Team and Physics Integration Unit 1999 *Nucl. Fusion* **39** 2137
[12] Loarte A. *et al* 2007 *Nucl. Fusion* **47** S203
[13] Creely J. *et al* 2020 *J. Plasma Phys.* **86** 865860502
[14] Schuster C.U. *et al* 2022 *Nucl. Fusion* **62** 026016
[15] Lennholm M. *et al* 2024 *Nucl. Fusion* **64** 096036
[16] Lennholm M. *et al* 2024 *Phil. Trans. R. Soc. A* **382** 20230403
[17] Romanelli M. *et al* 2014 *Plasma Fusion Res.* **9** 3403023
[18] Hawryluk R.J. *et al* 1980 *An Empirical Approach to Tokomak Transport Physics of Plasmas Close to Thermonuclear Conditions* ed B. Coppi *etal* vol 1 (CEC) pp 19–46
[19] Pankin A.Y., Breslau J., Gorelenkova M., Andre R., Grierson B., Sachdev J., Goliyad M. and Perumpilly G. 2025 *Comput. Phys. Commun.* **312** 109611
[20] Copi B. and Sharky N. 1981 *Nucl. Fusion* **21** 1363
[21] Garzotti L. *et al* 2003 *Nucl. Fusion* **43** 1829
[22] Zotta V. *et al* 2024 *50th EPS Conf. on Plasma Physics (EPS 2024)* (*Salamanca, Spain, 8–12 July 2024*) (available at: https://epsplasma2024.com/)
[23] Tala T. *et al* 2023 *Nucl. Fusion* **63** 112012
[24] Zotta V.K. *et al* 2022 *Nucl. Fusion* **62** 076024
[25] Pankin A., McCune D., Andre R., Bateman G. and Kritz A. 2004 The Tokomak Monte Carlo fast ion module NUBEAM in the national transport code collaboration library *Comput. Phys. Commun.* **159** 157–84
[26] Tamor S. 1981 *J. Comput. Phys.* **40** 104
[27] Cenacchi G. and Taroni A., 1988 *JET report JET-IR(88)03*
[28] Stubberfield P. and Watkins M. 1987 *JET report JET-DPA(06)/87*
[29] Challis C.D., Cordey J.G., Hamnén H., Stubberfield P.M., Christiansen J.P., Lazzaro E., Muir D.G., Stork D. and Thompson E. 1989 *Nucl. Fusion* **29** 563
[30] Hirvijoki E., Asunta O., Koskela T., Kurki-Suonio T., Miettunen J., Sipilä S., Snicker A. and Äkäslompolo S. 2014 *Comput. Phys. Commun.* **185** 1310
[31] Erba M., Cherubini A., Parail V.V., Springmann E. and Taroni A. 1997 *Plasma Phys. Control. Fusion* **39** 261
[32] JETTO wiki manual (available at: https://users.euro-fusion.org/pages/data-cmg/wiki/JETTO_Wiki.html)
[33] Garzotti L., Pegourie B., Geraud A., Frigione D. and Baylor L.R. 1997 *Nucl. Fusion* **37** 1167
[34] Koechl F. *et al* 2012 *JET report EFDA–JET–PR(12)57*
[35] Schneider P. *et al* 2023 *Nucl. Fusion* **63** 112010
[36] Weisen H. *et al* 2020 *J. Plasma Phys.* **86** 905860501
[37] Garcia J. *et al* 2022 *Plasma Phys. Control. Fusion* **64** 054001
[38] Bourdelle C., Camenen Y., Citrin J., Marin M., Casson F.J., Koechl F. and Maslov M. 2018 *Nucl. Fusion* **58** 076028
[39] Maslov M. *et al* 2018 *Nucl. Fusion* **58** 076022
[40] Schneider P. *et al* 2022 *Nucl. Fusion* **62** 026014
[41] IAEA Veinna 2012 *Fusion Physics* eds M. Kikuchi, K. Lackner and M.Q. Tang
[42] Angioni C., Fable E., Greenwald M., Maslov M., Peeters A.G., Takenaga H. and Weisen H. 2009 *Plasma Phys. Control. Fusion* **58** 124017
[43] Belli E.A. and Candy J. 2021 *Phys. Plasmas* **28** 062301
[44] Casson F. *et al* 2020 *Nucl. Fusion* **60** 066029
[45] Marin M., Citrin J., Bourdelle C., Camenen Y., Casson F.J., Ho A., Koechl F. and Maslov M. 2020 *Nucl. Fusion* **60** 046007
[46] Horton W. 1999 *Rev. Mod. Phys.* **71** 735
[47] Hannum D., Bateman G., Kinsey J., Kritz A.H., Onjun T. and Pankin A. 2001 *Phys. Plasmas* **8** 964
[48] Erba M., Aniel T., Basiuk V., Becoulet A. and Litaudon X. 1998 *Nucl. Fusion* **38** 1013
[49] Scott S.D. *et al* 1995 *Phys. Plasmas* **2** 2299
[50] Cordey J. *et al* 1999 *Nucl. Fusion* **39** 301
[51] Simonini R., Corrigan G., Radford G., Spence J. and Taroni A. 1994 *Contrib. Plasma Phys.* **34** 368
[52] Reiter D., Baelmans M. and Börner P. 2005 *Fusion Sci. Technol.* **47** 172
[53] Corrigan G. 2019 note on JETTO updates

[54] Leoni C. *et al* 2024 *50th EPS Conf. on Plasma Physics (EPS 2024)* (*Salamanca, Spain*, *8–12 July 2024*) (available at: https://epsplasma2024.com/)
[55] Lauro-Taroni L. *et al* 1994 *EPS Conf. on Controlled Fusion and Plasma Physics* (*Montpellier, France*, *27 June–1 July 1994*) vol 21 p 102
[56] Zotta V.K. *et al 48th EPS Conf. on Plasma Physics (EPS 2022)* (*27 June–1 July 2022*) (available at: https://epsplasma2022.eu/)
[57] Frassinetti L., Beurskens M.N.A., Scannell R., Osborne T.H., Flanagan J., Kempenaars M., Maslov M., Pasqualotto R. and Walsh M. 2012 *Rev. Sci. Instrum.* **83** 013506
[58] Ingesson L.C. 1999 *JET Report JET-R(99)06*
[59] Zoita V. *et al* 2009 *IEEE Int. Conf. on Plasma Science—Abstracts* (*San Diego, CA, USA*, *1–5 June 2009*) (available at: www.proceedings.com/06018.html)
[60] Ghani Z. *et al* 2018 *Fusion Eng. Des.* **136** 233
[61] Biewer T.M. *et al* 2007 *JET Report EFDA–JET–CP(07)03/24*
[62] Neverov V.S., Kukushkin A.B., Stamp M.F., Alekseev A.G., Brezinsek S. and von Hellermann M. 2017 *Nucl. Fusion* **57** 016031
[63] Maggi C.F. *et al* 2012 *Rev. Sci. Instrum.* **83** 10D517
[64] Lomanowski B.A., Meigs A.G., Conway N.J., Zastrow K.-D., Sharples R.M., Heesterman P. and Kinna D. 2014 *Rev. Sci. Instrum.* **85** 11E432
[65] Kruezi U., Sergienko G., Morgan P.D., Matthews G.F., Brezinsek S. and Vartanian S. 2012 *Rev. Sci. Intrum.* **83** 10D728
[66] Felton R. *et al* 2025 *Plasma Phys. Control. Fusion* accepted (https://doi.org/10.1088/1361-6587/ae0207)
[67] Angioni C. *et al* 2007 *Nucl. Fusion* **47** 1326
[68] Lao L., St. John H., Stambaugh R.D., Kellman A.G. and Pfeiffer W. 1985 *Nucl. Fusion* **25** 1611
[69] Stancar Ž. *et al* 2023 *Nucl. Fusion* **63** 126058
[70] Tholerus E. *et al* 2024 *Nucl. Fusion* **64** 106030
[71] Valovič M. *et al* 2019 *Nucl. Fusion* **59** 106047